In vitro reconstitution defines the mechanistic basis of HSET motor activity regulation by IntraFlagellar Transport proteins

Audrey Guesdon[1,2], Valérie Simon[1], Juliette Van Dijk[1], Bénédicte Delaval[1, *] and Benjamin Vitre[1, *]

[1] Centre de Recherche en Biologie cellulaire de Montpellier (CRBM), Univ Montpellier, CNRS, Montpellier, France
[2] Present Address: Centre de Biologie Structurale (CBS), Univ Montpellier, CNRS, Montpellier, France

* Co-corresponding authors :

Bénédicte Delaval
CRBM - CNRS - Université de Montpellier
1919, route de Mende
34293 - Montpellier Cedex 05 – France
email: benedicte.delaval@crbm.cnrs.fr

Benjamin Vitre
CRBM - CNRS - Université de Montpellier
1919, route de Mende
34293 - Montpellier Cedex 05 - France
email: benjamin.vitre@crbm.cnrs.fr

Running title: HSET regulation by IFT proteins.

Keywords: Kinesin regulation, mitosis, HSET, microtubules, IntraFlagellar Transport proteins, in vitro reconstitution.

Competing Interests: The authors declare no competing interests.

Abstract

HSET is a mitotic kinesin essential for centrosome clustering in cells harboring supernumerary centrosomes. Work *in cellulo* revealed that IntraFlagellar Transport proteins (IFT) interact with the kinesin HSET to promote efficient extra centrosome clustering and subsequent cancer cell proliferation. However, whether and how IFT proteins regulate HSET activity is unknown. Using a reconstituted *in vitro* system combining purified HSET and IFT proteins coupled to TIRF microscopy approaches, we identified a minimal subcomplex made of IFT52/IFT70 directly binding to HSET. We demonstrate that this binding induces HSET oligomerization allowing its activation and the formation of processive HSET complexes. We also show that HSET activation by IFT proteins accounts for an increased ability to slide microtubules and to organize dynamic microtubule networks *in vitro*. Overall, this work shows that IFT proteins can directly activate a mitotic kinesin and provides mechanistic explanation for the contribution of IFT proteins to efficient centrosome clustering.

Introduction

Mitotic spindle bipolarity is essential to ensure accurate segregation of the genetic material in the two daughter cells during cell division. In animal cells, the formation of a bipolar mitotic spindle requires the establishment of polarized radial arrays of microtubules focused around the spindle poles. Those arrays, or asters, are subsequently separated and stabilized in a bipolar structure through the contribution of mitotic motors and microtubules associated proteins (Valdez *et al*, 2023).

Microtubule focusing at the spindle poles depends on the microtubule minus-end directed motor dynein in association with NuMA (Heald *et al*, 1996; Merdes *et al*, 2000; Hueschen *et al*, 2017) and on the microtubule minus-end directed motors of the kinesin-14 family including Ncd in drosophila (Goshima *et al*, 2005) and HSET in human (Mountain *et al*, 1999). Kinesin-14 motors present conserved domain organization with an ATP-independent microtubule binding domain at their N-terminus, a coiled-coil domain in their central part and an ATP-dependent microtubule binding and motor domain at their C-terminus (She & Yang, 2017). *In vitro*, kinesin-14 motors display a minus end directed activity (Walker *et al*, 1990; McDonald *et al*, 1990; Mountain *et al*, 1999) and their two microtubule binding sites allow them to crosslink microtubules and focus their minus ends (Fink *et al*, 2009; Braun *et al*, 2017) favoring aster formation (Hentrich & Surrey, 2010). In cells, the contribution of kinesins 14 to spindle pole

formation and maintenance varies between organisms or cell type. For instance, Ncd is essential for aster formation and spindle pole focusing in drosophila mitotic cells (Goshima & Vale, 2003) and HSET is important for the assembly of acentrosomal mouse oocyte mitotic spindle (Mountain *et al*, 1999). If HSET has mild effects on mammalian somatic cell spindle size regulation (Cai *et al*, 2009), it becomes essential in cells harboring multiple centrosomes. Indeed, in cancer cells that frequently harbor supernumerary centrosomes (Chan, 2011) HSET is essential for extra centrosome clustering leading to pseudo-bipolar mitotic spindle organization (Kwon *et al*, 2008). Upon HSET depletion, cancer cells harboring supernumerary centrosomes failed to cluster their centrosomes leading to catastrophic mitotic errors and subsequent cell death (Kwon *et al*, 2008; Chavali *et al*, 2016).

Diverse mechanisms fine tuning the activity of kinesin-14 motor activity throughout mitosis were identified over the years. First, HSET abundance is regulated through Cdk1 dependent phosphorylation within a D-box at its N-terminus which prevents its degradation by APC/C^{CDH1} during early mitosis (Singh *et al*, 2014). Second, HSET motor activity *per se* can also be positively or negatively regulated. For example, Xenopus kinesin 14 XCTK2 activity is negatively regulated through its interaction with importins α/β (Guo *et al*, 2019; Ems-McClung *et al*, 2020). *In vitro*, individual HSET motility can be activated by low ionic strength (Furuta & Toyoshima, 2008) or by applying a traction force on them (Reinemann *et al*, 2018). Finally, HSET clustering or oligomerization either through its N-terminal tail binding to soluble tubulin (Norris *et al*, 2018) or through binding to a bead (Liu *et al*, 2024) was shown to activate its motility. Similarly, HSET oligomerization through its association with plus-end tracking protein Mal3 could promote its activity (Ogren *et al*, 2022).

Work in cells also identified IntraFlagellar Transport Proteins (IFT) as a novel class of proteins interacting and potentially modulating HSET activity to control efficient clustering of extra centrosome (Vitre *et al*, 2020). IFT proteins are primarily described to form large macromolecular complexes called IFT trains, that function as cargo adaptors of ciliary proteins (Lechtreck, 2022). *In vitro* work also identified regulatory roles for IFT proteins on ciliary motors since they can activate the C. elegans ciliary kinesin OSM-3 (Mohamed *et al*, 2018). However, the mechanisms of action of IFT proteins on HSET motor activity regulation remains unknown. Using *in vitro* reconstituted assays, we identify here a minimal IFT complex composed of IFT52/70 that directly interacts with the human kinesin HSET. This interaction activates the motor and stimulates its microtubule sliding activity. We also show that HSET activation upon

IFT binding enhances HSET bundling and clustering capacity, mechanistically explaining the cellular role of IFT proteins/HSET interaction observed *in cellulo* in the clustering of extra centrosomes (Vitre *et al*, 2020).

Results and discussion

HSET directly binds to a minimal IFT52/70 complex

We previously showed that human HSET can interact in vitro with a purified recombinant IFT88/70/52/46 subcomplex from Chlamydomonas reinhardtii origin (Vitre *et al*, 2020). To identify a minimal IFT complex interacting with HSET, we now purified mammalian SNAP-tagged IFT proteins from baculovirus-infected insect cells and tested their binding to recombinant GFP-HSET. Using GFP-trap pull down, we showed that a minimal complex made of IFT52/70 directly interacts with HSET (Fig. 1a and 1b). Another IFT, IFT46, weakly interacted with HSET (Fig. 1a and 1c) and was therefore used as a negative control in the subsequent functional experiments. To assess the stoichiometry of IFT52/70-HSET complex in solution we performed size exclusion chromatography coupled to multi-angle light scattering analysis (SEC-MALS). SEC-MALS analysis yielded a molecular mass for HSET of 217 kDa consistent with the calculated mass of 210 kDa expected for a dimeric motor (peak a, Fig1 d, e). Analysis of IFT52/70 alone yielded a molecular mass of 377 kDa (peak b, Fig1 d, e). Given the expected calculated molecular mass of 174 kDa for a complex of IFT52/70, this indicated that, at this concentration (1.7 mg/ml) IFT52/70 tends to oligomerize in solution. When IFT52/70 were incubated with HSET prior to SEC-MALS analysis, a peak (peak 1 Fig. 1d) was measured at 366 kDa corresponding to a complex of one IFT52/70 and one HSET dimer (expected mass of 384 kDa). The presence of both HSET and IFT52/70 was confirmed by SDS page analysis of the peak fraction (Fig. 1e). A second peak is observed for IFT52/70-HSET incubation with a measured molecular mass of 302 kDa (peak 2, Fig. 1d) likely corresponding to a complex made of a monomer of HSET and one IFT52/70 dimer (expected mass of 279 kDa). This hypothesis is consistent with the SDS page signals of the proteins observed in this peak which show a weaker signal of HSET compared to IFT52/70 contrarily to what is observed in peak 1 (Fig. 1e). Altogether, this biochemical analysis confirms that HSET and IFT52/70 directly interact in solution, with a stability sufficient to withstand the dilution occurring during the size exclusion chromatography.

IFT52/70 binding to HSET stimulates its processive activity through its oligomerization

To assess the impact of IFT52/70-HSET binding on motor activity we monitored the dynamic behavior of IFT52/70-HSET complex in an *in vitro* reconstituted assay using TIRF microscopy. GMPCPP stabilized microtubules were attached to coverslip in PLL-PEG passivated imaging chambers and HSET with or without IFT52/70 were flown-in to allow the observation of HSET or IFT-HSET complexes. As expected HSET alone mostly displayed a diffuse behavior with rapid bidirectional movement and frequent directional switch (Fig. 2a, Supplementary Fig. 1a and Movie 1). When HSET was incubated with IFT52/70 we observed processive particles containing both HSET and IFT52/70 (labelled with Alexa fluor 647 on their SNAP tag). This indicates that IFT proteins can interact with HSET when the kinesin is active on microtubules (Fig. 2a, b, Supplementary Fig1. a and Movies 2, 3). Importantly, quantification of these events showed that IFT52/70 binding to HSET significantly increased processive HSET runs with an average of 0.046± 0.001 processive event per µm of microtubules per minute compared to 0.012± 0.002 in HSET alone condition (Fig. 2b). Incubation of HSET with IFT46, which displayed weak binding to HSET (Fig. 1c), did not significantly increase the rate of processive events (Fig. 2b). This shows that IFT52/70 binding to HSET specifically activates the kinesin.

HSET oligomerization has been shown to increase its capacity to do processive runs (Norris *et al*, 2018; Liu *et al*, 2024). To test whether IFT52/70 binding to HSET could favor its activation through oligomerization, we measured the fluorescence intensity of processive HSET particles when HSET is alone or in the presence of IFT52/70. Fluorescence signal intensity measurements of a dimeric GFP-HSET (see methods and Supplementary Fig. 1b) were used to quantify the number of GFP molecules per active HSET particle. At the population level, IFT52/70 binding to HSET increased active particle median signal by 60 % (fluorescence intensity of 1357.5 a.u vs 2183.3; Supplementary Fig. 1c) suggesting that IFT favors HSET oligomerization. To visualize this effect at the level of individual particles, the distribution of particles according to the number of HSET dimer per particles was analyzed in a frequency distribution histogram (Fig. 2c). In the control condition the majority of processive particles contained one or two HSET dimer (91 particles corresponding to 68.9 % all processive particles) with the largest group containing a single HSET dimer (49 particles corresponding to 37.1 % of all processive particles). Strikingly, in presence of IFT52/70, the majority of processive particles contained more than two HSET dimers (380 particles corresponding to 52.3 % of all processive particles) indicating increased oligomerization in this condition.

Altogether, those data suggest that IFT52/70 stimulates HSET activation by favoring its oligomerization. This effect is consistent with the activation of HSET through its oligomerization by soluble free tubulin that was previously described (Norris *et al*, 2018).

IFT52/70 binding to HSET favors its directional activity and its accumulation at microtubules minus ends

We noticed that HSET particles frequently stayed connected to microtubule ends in the presence of IFT52/70 (Supplementary Fig. 1d). This suggested that IFT52/70 binding to HSET may favor HSET activation and directional movement toward one microtubule end. To test this hypothesis, we incubated 10 times more HSET with or without IFT52/70 and measured fluorescence intensity along microtubule length. At this higher HSET concentration, HSET clearly accumulated at one microtubule end leading to HSET comet formation (Fig. 2d,e). While a small accumulation of HSET was detected with the motor alone due to its occasional processivity (Fig. 2b), a 2-fold increase of HSET comet intensity was observed upon incubation with IFT52/70 (1.4 versus 2.8 fluorescence ratio unit to control lattice, Fig. 2f). This showed that IFT52/70 binding to HSET activates HSET processive run toward one microtubule end. To determine the directionality of HSET runs upon IFT52/70 binding, we successively injected Kip2-RFP a microtubule plus-end decorating kinesin (Chen *et al*, 2023) and HSET. As expected, HSET accumulated at the opposite end of Kip2-RFP, confirming its minus end accumulation (Supplementary Fig1.e). These results, using HSET and IFT at higher concentration, showed that IFT52/70 binding to HSET favors its processivity towards microtubule minus ends ultimately leading to comet formation.

IFT52/70 binding to HSET increases its bundling and sliding activity

Functionally, kinesins 14 are required to remodel microtubule networks by crosslinking/bundling and sliding anti-parallel microtubules towards their minus ends both in cells (Cai *et al*, 2009; Hepperla *et al*, 2014) and *in vitro* (Braun *et al*, 2009; Fink *et al*, 2009; Braun *et al*, 2017). We thus tested whether IFT52/70 binding to HSET could affect its bundling and sliding activity. To visualize microtubule bundling and sliding upon collective HSET activity, biotinylated GMPCPP stabilized microtubules dimly labelled with Atto565 were attached to the coverslip of the imaging chamber. Bright non-biotinylated microtubule seeds were then added with HSET alone (Fig. 3a, Supplementary Fig. 2a and movies 4, 5) or with HSET incubated

with IFT52/70 (Fig. 3a, Supplementary Fig. 2a and movies 6, 7) and monitored using TIRF microscopy. In the presence of IFT52/70, the total number of bright microtubule seeds bundled with dim template microtubules was significantly increased showing that IFT52/70 binding to HSET increased its bundling capacity by 30 % (0.043± 0.003 events per µm of template in the control versus 0.058± 0.004 with IFT52/70; Fig. 3b). Of note, IFT52/70 colocalized with HSET between bundled seeds indicating that IFT52/70 direct binding to HSET is maintained when HSET crosslinks adjacent microtubules (Supplementary Fig. 2b). Among the bundled seeds, IFT52/70 binding to HSET also strongly increased the number of mobile seeds sliding on template microtubules (70% increased from 0.018± 0.001 events per µm of template in the control to 0.031± 0.002 in the condition with IFT52/70; Fig. 3c). The average speed of those moving seeds also increased in the presence of IFT52/70 with a distribution of individual seed speed shifted to higher values and an average seed speed increased by 40 % (0.458± 0.02 µm/min in the control versus 0.650± 0.02 µm/min with IFT52/70; Fig. 3d). Previous studies have shown that microtubule gliding or sliding speed can be differentially impacted depending on the concentration or density of HSET (Braun *et al*, 2017; Liu *et al*, 2024), XCTK2 (Hentrich & Surrey, 2010) or Ncd (Kaneko *et al*, 2020) present in the assay. We thus tested whether higher density of HSET motor in the presence of IFT proteins could account for this increased bundling and sliding capacity. To quantify HSET density on sliding microtubule seeds, we measured the ratio of GFP-HSET fluorescence signal to tubulin Atto565 signal (Fig. 3e) and showed that HSET accumulates at higher density on sliding microtubules in presence of IFT52/70 (ratio value of 0.43± 0.13 in control versus 0.56± 0.20 with IFTs). Altogether, these results show that IFT52/70 direct binding to HSET increases its bundling and sliding capacity and correlates with a higher density of motors. These results are also consistent with the increased motor activity observed at the single particle level (Fig. 2).

IFT52/70 binding to HSET favors the formation of active microtubule networks

Minus-end accumulation of motor proteins such as dynein (Tan *et al*, 2018; Foster *et al*, 2015) or HSET (Roostalu *et al*, 2018) favors large scale microtubule network organizations into polarized aster structures. Moreover, it was shown experimentally and by simulation that crosslinking and sliding of microtubule minus-end-directed-motors such as HSET favors the formation of active microtubule networks that eventually evolve towards asters over time depending on motor and microtubule concentrations (Roostalu *et al*, 2018; Henkin *et al*, 2022; Chew *et al*, 2023;

Hentrich & Surrey, 2010). We thus tested whether the increased accumulation of HSET at microtubule minus ends (Fig. 2) together with the increased sliding activity of HSET (Fig. 3) in the presence of IFT52/70 could increase HSET ability to organize active microtubule networks. Using an *in vitro* active microtubule network assay that can be monitored at low resolution (10 x objective), we showed that active microtubule network organization by HSET is increased in the presence of IFT52/70. Indeed, while microtubule bundles were already visible at the first imaging time point, one minute after mixing the components both in control and IFT52/70 conditions (Fig. 4a and movies 8, 9), they organized more rapidly into contractile microtubule networks (Fig. 4a, 10 min) and evolved faster towards radial microtubule organization or aster like structures in presence of IFT52/70 (Fig. 4a, 30 min)). This can be precisely quantified by measuring overall image contrast over time which is a readout of microtubule structure compaction (Hentrich & Surrey, 2010). In all conditions, contrast increased over time reflecting the microtubule network compaction before tending towards a plateau at 30 minutes indicating a steady state in the network organization (Fig. 4b). However, increased compaction (i.e. more bundles) was already observed at the first timepoint (1 min after mixing the components) in the presence of IFT52/70 (1.017± 0.027 contrast a.u. in control versus 1.39± 0.057 with IFT52/70) and continuously increased until 30 minutes (2.68± 0.21 contrast a.u. in control versus 4.49± 0.27 with IFT52/70) reflecting a faster and stronger organization of the active microtubule network into aster-like structures in the presence of IFT52/70. We then measured the slopes of the linear parts of the curves as a proxy of microtubule network compaction speed (Fig. 4c) and found that the presence of IFT52/70 increased 2.3 times microtubule compaction speed (slopes going from 0.07 to 0.16) confirming the faster contraction. To further control for specificity and ensure that protein crowding alone was not responsible for the observed effect, we used IFT46 that does not increase HSET activity (Fig. 2) and SNAP tag as controls. A minimal effect of IFT46 and SNAP was observed with an increased compaction speed of only 0.6 time (Fig. 4c) indicating that protein crowding may slightly influence compaction but confirming the specificity of HSET activation by IFT52/70. Importantly, HSET and IFT52/70 are present along the contractile microtubule network and accumulate at the center of the asters by the end of the imaging period (Fig. 4d) consistent with a role of their minus-end accumulation in active network organization and aster-like structure formation.

Altogether, using purified proteins and *in vitro* reconstituted assays, these results show that

IFT52/70 directly binds to HSET (Fig.1) and that this interaction increases HSET motor activity through oligomerization of the motors (Fig. 2, Supplementary Fig. 3a). While IFT proteins have been shown to regulate the C.elegans ciliary kinesin 2 OSM-3 (Mohamed *et al*, 2018) this work is the first demonstration of the regulation of a human mitotic kinesin by IFT proteins. HSET activation by oligomerization was previously observed via diverse mechanisms including oligomerization with tubulin forming clusters containing multiple tubulin dimers and HSET dimers (Norris *et al*, 2018). Similarly, binding of multiple HSET to a single quantum dot can also favor HSET activity. In solution we found HSET dimer bound to IFT52/70 with a one-to-one ratio and we also found that IFT52/70 dimer could oligomerize (Fig.1). Thus, it is possible that when HSET-IFT52/70 complexes contact the microtubule, interaction between HSET bound IFT52/70 proteins favors their oligomerization. This hypothesis is consistent with recent in situ Cryo-EM characterization of anterograde IFT train in Chlamydomonas cilia indicating that lateral interaction between IFT52/70/88 are mediating the lateral interaction in the trains (Lacey *et al*, 2023). We did also quantify numerous events of single HSET dimer bound to IFT52/70 doing processive runs. We thus cannot exclude that part of the activating effects of IFT proteins on HSET can be driven by other mechanisms than oligomerization. Low ionic strength (5 µM KAc) has been proposed to increase HSET motor activity (Furuta & Toyoshima, 2008) but it is likely not the case here since our experiments were done at a conventional concentration of 50 µM KCl in absence or presence of IFT52/70. Another mechanism regulating kinesin activity is autoinhibition (Verhey & Hammond, 2009). Some previous works proposed that HSET might not be inhibited by head to tail interaction since a persistent absence of motor activity was observed when its N-terminal tail was removed (Norris *et al*, 2018) or because it appears in "open" conformation when observed by electron microscopy (Sturgill *et al*, 2014). However, other data could favor an autoinhibition hypothesis. For example, for the kinesin 14 motor Ncd, it was recently shown that its N-terminal tail interacts with its motor domain and that NuMA's fly ortholog Mud could relieve this interaction (Cutillas & Johnston, 2021). We have previously shown that IFT88/70/52/46 complex interacts with HSET C-terminal part containing its motor domain (Vitre *et al*, 2020). It is thus possible that IFT52/70 binding to HSET prevents its autoinhibition but further biochemical and/or structural biology work will be necessary to assess this hypothesis.

Our study also demonstrates that the increased HSET activity upon IFT52/70 binding resulted in HSET accumulation at microtubule minus ends (Fig. 2 and Supplementary Fig. 3b) as well

as an increased ability to slide microtubules (Fig. 3 and Supplementary Fig. 3c). Those two mechanisms have been described to drive different organization of active microtubule networks with end-binding favoring aster formation while sliding favors contractile bundle formation (Hentrich & Surrey, 2010; Roostalu *et al*, 2018; Chew *et al*, 2023). Indeed, when we assessed the effect of IFT52/70 bound HSET on microtubule network organization we observed first the formation of contractile networks that evolved towards asters over time (Fig. 4 and supplementary Fig. 3d). This transition is driven by the equilibrium between the concentration of microtubules and the density of motors present in the experimental chamber as demonstrated using simulation (Henkin *et al*, 2022; Chew *et al*, 2023) and IFT52/70 activation of HSET only speeds up the process. Of note, it was previously shown that increased density of kinesins 14 along sliding or gliding microtubules tend to slow down the moving seed speed potentially due to non-specific interaction of the kinesin N-terminal tails with microtubules (Hentrich & Surrey, 2010; Braun *et al*, 2017; Liu *et al*, 2024). This effect seems contradictory to our observations, but it was shown in a range of concentrations below 25 nM and tends to be reversed above 50 nM (Hentrich & Surrey, 2010) which is consistent with our observations.

Interestingly this increased activity of HSET bound to IFT52/70 leading to the coalescence of multiple microtubule seeds into polarized structures is reminiscent of the regulatory role of IFT proteins in HSET dependent clustering of extra centrosomes we described previously in cells (Vitre *et al*, 2020). The *in vitro* set up used here thus allows to mimic and mechanistically explain, using a bottom up approach, the phenotype previously described *in cellulo* regarding the regulatory activity of IFT proteins on HSET motor activity (Supplementary Fig. 3e).

Since extra centrosomes are frequently found in cancer while they are extremely rare in normal cycling cells, targeting HSET activity has appeared as a good strategy to specifically kill cancer cells (Ogden *et al*, 2012). Specific inhibitor of HSET ATPase activity were thus developed showing efficacy *in cellulo* (Watts *et al*, 2013; Wu *et al*, 2013; Zhang *et al*, 2016). However, inhibitors of kinesins that target their ATPase activity often have off target activity, and resistance due to the appearance of point mutations is a substantial drawback in the development of such inhibitors (Myers & Collins, 2016). Targeting regulatory proteins that interact with kinesins to inhibit specific functions appears as an attractive therapeutic alternative and small molecule perturbing IFT protein-HSET interaction could be a novel way to modulate HSET activity.

References

Braun M, Drummond DR, Cross RA & McAinsh AD (2009) The kinesin-14 Klp2 organizes microtubules into parallel bundles by an ATP-dependent sorting mechanism. *Nat Cell Biol* 11: 724–730

Braun M, Lansky Z, Szuba A, Schwarz FW, Mitra A, Gao M, Lüdecke A, Ten Wolde PR & Diez S (2017) Changes in microtubule overlap length regulate kinesin-14-driven microtubule sliding. *Nat Chem Biol* 13: 1245–1252

Cai S, Weaver LN, Ems-McClung SC & Walczak CE (2009) Kinesin-14 family proteins HSET/XCTK2 control spindle length by cross-linking and sliding microtubules. *Mol Biol Cell* 20: 1348–1359

Castoldi M & Popov A V (2003) Purification of brain tubulin through two cycles of polymerization–depolymerization in a high-molarity buffer. *Protein Expr Purif* 32: 83–88

Chan JY (2011) A clinical overview of centrosome amplification in human cancers. *Int J Biol Sci* 7: 1122–1144

Chavali PL, Chandrasekaran G, Barr AR, Tátrai P, Taylor C, Papachristou EK, Woods CG, Chavali S & Gergely F (2016) A CEP215-HSET complex links centrosomes with spindle poles and drives centrosome clustering in cancer. *Nat Commun* 7: 11005

Chen X, Portran D, Widmer LA, Stangier MM, Czub MP, Liakopoulos D, Stelling J, Steinmetz MO & Barral Y (2023) The motor domain of the kinesin Kip2 promotes microtubule polymerization at microtubule tips. *Journal of Cell Biology* 222

Chew WX, Henkin G, Nédélec F & Surrey T (2023) Effects of microtubule length and crowding on active microtubule network organization. *iScience* 26

Cutillas V & Johnston CA (2021) Mud binds the kinesin-14 Ncd in Drosophila. *Biochem Biophys Rep* 26: 101016

Ems-McClung SC, Emch M, Zhang S, Mahnoor S, Weaver LN & Walczak CE (2020) RanGTP induces an effector gradient of XCTK2 and importin α/β for spindle microtubule cross-linking. *Journal of Cell Biology* 219: 1–15

Fink G, Hajdo L, Skowronek KJ, Reuther C, Kasprzak AA & Diez S (2009) The mitotic kinesin-14 Ncd drives directional microtubule-microtubule sliding. *Nat Cell Biol* 11: 717–723

Foster PJ, Furthauer S, Shelley MJ & Needleman DJ (2015) Active contraction of microtubule networks. *Elife* 4: 1–21

Furuta K & Toyoshima YY (2008) Minus-End-Directed Motor Ncd Exhibits Processive Movement that Is Enhanced by Microtubule Bundling In Vitro. *Current Biology* 18: 152–157

Goshima G, Nédélec F & Vale RD (2005) Mechanisms for focusing mitotic spindle poles by minus end-directed motor proteins. *Journal of Cell Biology* 171: 229–240

Goshima G & Vale RD (2003) The roles of microtubule-based motor proteins in mitosis: Comprehensive RNAi analysis in the Drosophila S2 cell line. *Journal of Cell Biology* 162: 1003–1016

Gradia SD, Ishida JP, Tsai M, Jeans C, Tainer JA & Fuss JO (2017) MacroBac : New Technologies for Robust and Efficient Large-Scale Production of Recombinant Multiprotein Complexes 1st ed. Elsevier Inc.

Guo L, Mohd KS, Ren H, Xin G, Jiang Q, Clarke PR & Zhang C (2019) Phosphorylation of importin-α1 by CDK1-cyclin B1 controls mitotic spindle assembly. *J Cell Sci* 132

Heald R, Tournebize R, Blank T, Sandaltzopoulos R, Becker P, Hyman A & Karsenti E (1996) Self-organization of microtubules into bipolar spindles around artificial chromosomes in Xenopus egg extracts. *Nature* 382: 420–425

Henkin G, Chew WX, Nédélec F & Surrey T (2022) Cross-linker design determines microtubule network organization by opposing motors. *Proc Natl Acad Sci U S A* 119: 1–12

Hentrich C & Surrey T (2010) Microtubule organization by the antagonistic mitotic motors kinesin-5 and kinesin-14. *Journal of Cell Biology* 189: 465–480

Hepperla AJ, Willey PT, Coombes CE, Schuster BM, Gerami-Nejad M, McClellan M, Mukherjee S, Fox J, Winey M, Odde DJ, *et al* (2014) Minus-end-directed kinesin-14 motors align antiparallel microtubules to control metaphase spindle length. *Dev Cell* 31: 61–72

Hirst WG, Kiefer C, Abdosamadi MK, Schäffer E & Reber S (2020) In Vitro Reconstitution and Imaging of Microtubule Dynamics by Fluorescence and Label-free Microscopy. *STAR Protoc* 1

Hueschen CL, Kenny SJ, Xu K & Dumont S (2017) NuMA recruits dynein activity to microtubule minus-ends at mitosis. *Elife* 6: 1–26

Hyman A, Drechsel D, Kellogg D, Salser S, Sawin K, Steffen P, Wordeman L & Mitchison T (1991) Preparation of modified tubulins. *Methods Enzymol* 196: 478–85

Kaneko T, Furuta K, Oiwa K, Shintaku H, Kotera H & Yokokawa R (2020) Different motilities of microtubules driven by kinesin-1 and kinesin-14 motors patterned on nanopillars. *Sci Adv* 6: 1–12

Kwon M, Godinho SA, Chandhok NS, Ganem NJ, Azioune A, Thery M & Pellman D (2008) Mechanisms to suppress multipolar divisions in cancer cells with extra centrosomes. *Genes Dev* 22: 2189–2203

Lacey SE, Foster HE & Pigino G (2023) The molecular structure of IFT-A and IFT-B in anterograde intraflagellar transport trains. *Nat Struct Mol Biol* 30: 584–593

Lechtreck K (2022) Cargo adapters expand the transport range of intraflagellar transport. *J Cell Sci* 135

Liu X, Rao L, Qiu W, Berger F & Gennerich A (2024) Kinesin-14 HSET and KlpA are non-processive microtubule motors with load-dependent power strokes. *Nat Commun* 15

McDonald HB, Stewart RJ & Goldstein LS (1990) The kinesin-like ncd protein of Drosophila is a minus end-directed microtubule motor. *Cell* 63: 1159–1165

Merdes A, Heald R, Samejima K, Earnshaw WC & Cleveland DW (2000) Formation of spindle poles by dynein/dynactin-dependent transport of NuMA. *Journal of Cell Biology* 149: 851–861

Mohamed MAA, Stepp WL & Ökten Z (2018) Reconstitution reveals motor activation for intraflagellar transport. *Nature* 557: 387–391

Mountain V, Simerly C, Howard L, Ando A, Schatten G & Compton DA (1999) The kinesin-related protein, HSET, opposes the activity of Eg5 and cross-links microtubules in the mammalian mitotic spindle. *Journal of Cell Biology* 147: 351–365

Myers SM & Collins I (2016) Recent findings and future directions for interpolar mitotic kinesin inhibitors in cancer therapy. *Future Med Chem* 8: 463–489

Norris SR, Jung S, Singh P, Strothman CE, Erwin AL, Ohi MD, Zanic M & Ohi R (2018) Microtubule minus-end aster organization is driven by processive HSET-tubulin clusters. *Nat Commun* 9: 1–14

Ogden a, Rida PCG & Aneja R (2012) Let's huddle to prevent a muddle: centrosome declustering as an attractive anticancer strategy. *Cell Death Differ* 19: 1255–67

Ogren A, Parmar S, Mukherjee S, Gonzalez SJ, Plooster M, McClellan M, Mannava AG, Davidson E, Davis TN & Gardner MK (2022) Kinesin-14 motors participate in a force balance at microtubule plus-ends to regulate dynamic instability. *Proc Natl Acad Sci U S A* 119

Reinemann DN, Norris SR, Ohi R & Lang MJ (2018) Processive Kinesin-14 HSET Exhibits Directional Flexibility Depending on Motor Traffic. *Current Biology* 28: 2356-2362.e5

Roostalu J, Rickman J, Thomas C, Nédélec F & Surrey T (2018) Determinants of Polar versus Nematic Organization in Networks of Dynamic Microtubules and Mitotic Motors. *Cell* 175: 796-808.e14

She ZY & Yang WX (2017) Molecular mechanisms of kinesin-14 motors in spindle assembly and chromosome segregation. *J Cell Sci* 130: 2097–2110

Singh SA, Winter D, Kirchner M, Chauhan R, Ahmed S, Ozlu N, Tzur A, Steen JA & Steen H (2014) Co-regulation proteomics reveals substrates and mechanisms of APC/C-dependent degradation. *EMBO Journal* 33: 385–399

Sturgill EG, Das DK, Takizawa Y, Shin Y, Collier SE, Ohi MD, Hwang W, Lang MJ & Ohi R (2014) Kinesin-12 kif15 targets kinetochore fibers through an intrinsic two-step mechanism. *Current Biology* 24: 2307–2313

Tan R, Foster PJ, Needleman DJ & McKenney RJ (2018) Cooperative Accumulation of Dynein-Dynactin at Microtubule Minus-Ends Drives Microtubule Network Reorganization. *Dev Cell* 44: 233-247.e4

Valdez VA, Neahring L, Petry S & Dumont S (2023) Mechanisms underlying spindle assembly and robustness. *Nat Rev Mol Cell Biol* 24: 523–542

Verhey KJ & Hammond JW (2009) Traffic control: regulation of kinesin motors. *Nat Rev Mol Cell Biol* 10: 765–777

Vitre B, Taulet N, Guesdon A, Douanier A, Dosdane A, Cisneros M, Maurin J, Hettinger S, Anguille C, Taschner M, *et al* (2020) IFT proteins interact with HSET to promote supernumerary centrosome clustering in mitosis. *EMBO Rep* 21: e49234

Walker RA, Salmon ED & Endow SA (1990) The Drosophila claret segregation protein is a minus-end directed motor molecule. *Nature* 347: 780–782

Watts CA, Richards FM, Bender A, Bond PJ, Korb O, Kern O, Riddick M, Owen P, Myers RM, Raff J, *et al* (2013) Design, synthesis, and biological evaluation of an allosteric inhibitor of HSET that targets cancer cells with supernumerary centrosomes. *Chem Biol* 20: 1399–1410

Wu J, Mikule K, Wang W, Su N, Petteruti P, Gharahdaghi F, Code E, Zhu X, Jacques K, Lai Z, *et al* (2013) Discovery and mechanistic study of a small molecule inhibitor for motor protein KIFC1. *ACS Chem Biol* 8: 2201–2208

Zhang W, Zhai L, Wang Y, Boohaker RJ, Lu W, Gupta V V., Padmalayam I, Bostwick RJ, White EL, Ross LJ, *et al* (2016) Discovery of a novel inhibitor of kinesin-like protein KIFC1. *Biochemical Journal* 473: 1027–1035

Material and methods

Protein expression and purification

GFP-HSET was expressed in Sf9 insect cells and purified as described in (Braun *et al*, 2017). Briefly, full-length N-terminal hexa-histidine-tagged GFP-HSET cloned in pOET1C-modified vectors (gift of S. Diez, TU Dresden) was expressed in Sf9 insect cells by infecting them with the appropriate baculovirus for 48h. Harvested cells were resuspended in lysis buffer (20 mM Hepes pH 7.2, 300 mM NaCl, 2 mM $MgCl_2$, 10 mM B-mercaptoethanol, 10 % glycerol, 0.5 % Triton X100, 50 µg/ml DNAse I, 1 mM PMSF, EDTA-free protease inhibitors (cOmplete Roche), 20 mM imidazole and 0.1 mM Mg-ATP). Cells were lysed using dounce homogenization and crude lysates were centrifuged at 75 000g for 45 min at 4 °C (25 000 rpm, Type 50.2 Ti rotor Beckman), loaded on Ni-NTA resin (Qiagen, 750 µl for 100 ml of cells) and incubated for 1h at 4 °C. The resin was washed for 2h with HSET purification buffer (20 mM Hepes pH 7.2, 300 mM NaCl, 2 mM $MgCl_2$, 5 mM B-mercaptoethanol, 100 µM Mg-ATP, 10 % glycerol) containing 30 mM imidazole. Proteins were eluted in HSET purification buffer containing 200 mM imidazole (70 µl elution buffer for 100 µl resin). For IFT proteins, cDNA of hIFT46, mIFT52 and hITF70 were cloned in 438-SNAP-V1 (addgene 55222) vector using LIC cloning as in (Gradia *et al*, 2017). IFT52 and IFT70 were cloned in the same vector with their own polyhedrin promoter so they could be co-expressed together. Both IFT52 and IFT70 have a twin strep tag and a SNAP tag. Baculoviruses were obtain using the pFastBac system. Proteins were expressed in Sf9 cells by infecting them with the appropriate baculovirus for 48h. Harvested cells were resuspended in lysis buffer (20 mM Hepes pH 7.2, 300 mM NaCl, 2 mM $MgCl_2$, 10 mM B-mercaptoethanol, 10 % glycerol, 0.5 % Triton X100, 50 µg/ml DNAse I, 1 mM PMSF, EDTA-free protease inhibitors (cOmplete Roche) supplemented with 0.1 mg/ml avidin. Cells were lysed using dounce homogenization and crude lysates were centrifuged at 75 000g for 45 min at 4 °C (25 000 rpm, Type 50.2 Ti rotor Beckman). Clear lysates were loaded on Streptactin resin (100 µl for 100 ml of cells, StrepTactin Sepharose High Performance Cytiva) and incubated for 1h30 at 4 °C. The resin was washed with wash buffer (20 mM Hepes pH 7.2, 300 mM NaCl and 1 M NaCl, 2 mM $MgCl_2$, 5 mM B-mercaptoethanol, 10 % glycerol) and proteins were eluted (strep tag cleavage by HRV-3C) and labelled simultaneously by incubating the resin O/N at 4 °C in elution buffer (20 mM Hepes pH 7.2, 300 mM NaCl, 2 mM $MgCl_2$, 1 mM DTT, 10 % glycerol; 100 µl for 100 µl resin) supplemented with HRV 3C protease (Pierce, 30 units for 100 µl elution buffer) and fluorescent dye SNAP-Surface Alexa Fluor 647 (NEB). Eluates were finally loaded on a biotin and dye removal spin column (Zeba, Thermo). Proteins were snap frozen in liquid nitrogen and stored at -80 °C until use. Protein size, purity and concentration were checked and measured on SDS-PAGE gel. Tubulin was purified from porcine brain using the high molar Pipes buffer protocol (Castoldi & Popov, 2003). Purified tubulin was labelled with fluorescent dye or biotin using standard protocols from Mitchison's

Lab (Hyman *et al*, 1991). Kip2-RFP was a gift from D. Portran expressed and purified as in (Chen *et al*, 2023).

GFP trap Pull down assays

9 µg of purified His-HSET or His-GFP were incubated on 40 µl of GFP-trap beads for 1h at 4 °C. 10 µl of beads were then incubated with IFT proteins (0.47 µM) in 20 mM Hepes pH 7.2, 75 mM NaCl, 2 mM $MgCl_2$, 1 mM DTT, for 2h at RT. Beads were washed 4 times and resuspended in Laemmli buffer for SDS-PAGE analysis. The IFT incubation flow through was collected and 47 % were loaded on SDS-PAGE gel.

SEC-MALS

Size exclusion chromatography – Multi-angle light scattering (SEC-MALS) experiments were performed at 25 °C, using a Superose 6 Increase 10/300 GL column connected to an AgilentTM Infinity II HPLC system combined to a miniDAWN TREOS light scattering detector (Wyatt TM) and an Optilab T-rEX differential refractive index detector (Wyatt TM). The column was equilibrated in 20 mM Na-Hepes pH 7.2, 300 mM NaCl, 2 mM $MgCl_2$, 5 % glycerol, 5 mM TCEP buffer. Bovine serum albumin was used as a calibration standard. IFT dimer and HSET samples were concentrated before SEC-MALS analysis to 29 and 35 µM, respectively, and incubated for 30 min at 30 °C before injection. Data acquisition and analyses were performed using the ASTRA 8 software (Wyatt).

TIRF microscopy chamber preparation

Experiments were performed in flow chambers assembled from a coverslip (Corning Cover glass Thickness ½ 24x50 mm; Cat No. 2980-245) attached to a glass slide (Knittel glass Starfrost 76x26 mm) with double-sided tape (NITTO cat EST-805, 50 µm thick). Flow chamber volumes were ranging from 5 to 8 µl depending on chamber width. Coverslips and glass slides were washed by sonicating in an isopropanol bath for 10 min, extensively rinsed with milliQ water (at least 10 “Hellendahl staining tank” volumes) and dried with argon. This step was followed by a plasma cleaning. Chambers were then passivated using PLL-PEG biotin (SuSos, 50 % labelled at 0.2 mg/ml final) for 5 minutes, washed with 2 to 3 volumes of BRB80 (1x), then flushed with neutravidin (0.25 mg/ml final) and incubated for 5 min. The chambers were finally washed with 2 to 3 volumes of BRB80 (1x) before injecting stabilized microtubules and the reaction mixture.

Seed preparation for *in vitro* reconstituted assays

For HSET single particle dynamic assays and sliding assays, GMPCPP stabilized and biotinylated dimly labelled microtubules (i.e template microtubules containing 20 % biotin

tubulin (0.6 µM) and 3 % Atto 565 tubulin (0.09 µM)) and non-biotinylated bright microtubules (i.e transported microtubules seeds containing 13 % of Atto 565 tubulin (2 µm)) were prepared as previously described (Hirst *et al*, 2020). For active microtubule network assays, taxol-stabilized microtubules were prepared using a protocol adapted from the Mitchison lab to obtain a microtubule seed stock at a concentration of 25 µM tubulin.

Single particle assay

HSET was incubated for 30 min at 30 °C with or without IFT proteins in 150 mM NaCl Hepes buffer (purification buffer) at a concentration of 0.75 µM for HSET and 1.5 µM for IFT proteins. Template biotinylated microtubules in BRB80 were flushed into the chamber and incubated for 5 min in order to attach to the coverslip. Incubated proteins were flushed in the chamber in a reaction mix containing 20 mM NaPIPES pH 6.8, 1 mM EGTA, 7.5 mM $MgCl_2$, 5 mM MgATP, 50 mM KCl, 1.5 mM GTP, 200 mM sucrose, 2 µM taxol, 0.25 mg/ml k-casein, 0.25 µM glucose oxydase, 0.064 µM catalase, 40 mM D-glucose, 17.5 mM beta-mercaptoethanol. Final concentrations of proteins in single particle assay were 0.5 nM HSET, 1 nM IFT52/70 and in the minus-end comet formation assay, 5 nM for HSET and 10 nM for IFT52/70. Image acquisition was performed using an inverted Nikon wide-field microscope equipped with a ILAS2 TIRF module (Roper), a 100X Plan TIRF Apochromat 1.49NA oil objective, an EMCCD iXon 897 Ultra Andor camera (512*512, 16µm pixel size) detector, controlled by Metamorph (Multi-dimensional acquisition module). Images were acquired every 1.4 sec for 7.5 minutes in the 3 channels (488, 561, 642). For the minus end comet formation assay, after 2 minutes of incubation images were also acquired with 1.4 sec interval but only the first image was used for further quantification.

Microtubule sliding assay

HSET was incubated for 30 min at 30 °C with or without IFT proteins in 150 mM NaCl Hepes buffer (purification buffer) at a concentration of 0.75 µM for HSET and 1.5 µM for IFT proteins. Template biotinylated microtubules in BRB80 were flushed into the chamber and incubated for 5 min in order to attach to the coverslip. Incubated proteins were added to non-biotinylated microtubules in a reaction mix containing 20 mM NaPIPES pH 6.8, 1 mM EGTA, 7.5 mM $MgCl_2$, 5 mM MgATP, 50 mM KCl, 1.5 mM GTP, 200 mM sucrose, 2 µM taxol, 0.25 mg/ml k-casein, 0.25 µM glucose oxydase, 0.064 µM catalase, 40 mM D-glucose, 17.5 mM beta-mercaptoethanol, and injected in the chamber containing template microtubules. Final concentrations of proteins in the assay were 50 nM HSET, 100 nM IFT dimer, 120 nM biotinylated seeds, and 150 nM non-biotinylated seeds. Image acquisition was performed using an inverted Nikon wide-field microscope equipped with a ILAS2 TIRF module (Roper), a 100X Plan TIRF Apochromat 1.49NA oil objective, an EMCCD iXon 897 Ultra Andor camera

(512*512, 16µm pixel size) detector, controlled by Metamorph (Multi-dimensional acquisition module). Images were acquired every minute for 30 minutes in the 3 channels (488, 561, 642). Three positions per condition were registered, all conditions were acquired in parallel chambers, at the same time.

Microtubule active network formation assays

Experiments were performed in similar flow chambers than TIRF experiments (without coating for passivation). HSET (0.75 µM) was incubated with or without IFT52/70, IFT46 or SNAP (1,5 µM) at 30 °C for 30 min, in Hepes buffer (purification buffer) containing a final concentration of 150 mM NaCl. The assay mix was prepared as following at room temperature: at the end of the incubation time, the appropriate volume of incubated sample was added to taxol -stabilized microtubule seeds, the sample was thoroughly mixed by pipetting up and down and quickly flushed into the chamber. Chambers were sealed with grease before acquisition. Images for all conditions (HSET alone, HSET/SNAP, and HSET/IFT proteins conditions) were acquired at the same time in parallel chambers. The final concentrations used in the assay were 100 nM HSET, 200 nM IFT dimer, IFT46 and SNAP, and the equivalent of 2.5 µM tubulin of taxol stabilized seeds in an assay buffer containing 20 mM NaPIPES pH 6.8, 1 mM EGTA, 7.5 mM $MgCl_2$, 5 mM MgATP, 50 mM KCl, 1.5 mM GTP, 200 mM sucrose, 2 µM taxol; 0.25 mg/ml k-casein, 0.25 µM glucose oxydase, 0.064 µM catalase, 40 mM D-glucose, 17.5 mM Bmercaptoethanol. Imaging was performed at 32 °C using an Inverted Nikon Ti-E wide-field microscope, a 10X Plan Apochromat 0.45NA air objective, and a sCMOS back-illuminated Prime95B Photometrics camera (1200*1200, 11 µm pixel size), controlled by NIS Elements (Nikon). Time-lapse wide-field fluorescence images were acquired at 1 min interval for a total duration of 30 min (31 frames). Three fields of view per chamber/condition were acquired on the appropriate channels.

Minus-end directed movement determination

The study of the directionality of HSET-IFT protein complex was performed on fluorescent GMPCPP microtubules using TIRF microscopy. Microtubule seeds were first incubated into an observation chamber, in order to adhere to the coverslip. The plus end directed kinesin Kip2 was flushed into the chamber and incubated for 5 to 10 min at 30 °C in order to allow the formation of comets at microtubule plus ends. The chamber was then washed with BRB80 to remove excess of Kip2, before flushing preformed HSET-IFT52/70 complex diluted in microtubule self-organization assay buffer, at a final concentration of 50 and 100 nM, respectively. One image per second was acquired during 5 min to observe the formation of HSET-IFT comets at microtubule minus end (opposite end than Kip2 accumulation).

Image Analysis

Image processing and analysis (cropping, rotating, brightness and contrast adjustment, color combining, and measurements) were performed using Fiji (ImageJ). For single particle analysis, kymograph of individual microtubules and velocity parameters were obtained using ImageJ Velocity Measurement Tool. Individual particle fluorescence (Supplementary Fig. 1c) is the average of the fluorescence signal of the first five time-intervals of each processive run. Values were corrected for background signal. To determine the number of GFP particles per track we first analyzed the average fluorescence decay of GFP-HSET particle attached to the imaging chamber that would bleach in one or two steps. The average intensity of particle that bleach in two steps was measured and set at 750 a.u. (Supplementary Fig. 1b). Individual fluorescence values of processive particles were divided by this value to determine the number of GFP-HSET dimer per moving particle (Fig. 2c). For sliding assays, the number of transport microtubules attached to and moving along template microtubules was measured manually. Sliding velocity was measured on kymographs, generated semi automatically with a homemade ImageJ macro including the plugin Kymograph Builder, and using the ImageJ Velocity measurement tool. Average fluorescence intensity of sliding microtubule was measured in the 488 and 561 channels using ROI overlapping the entire length of the moving seeds. The ratio of HSET signal to tubulin signal was calculated. This ratio was corrected with a correction factor corresponding to the ratio of HSET to tubulin on template microtubules without moving seeds, in the control condition, to take into account potential fluorescence signal variation in the two channels between different experiments. For active_microtubule network assay image contrast was defined as the standard deviation of the fluorescent signal that was measured on the tubulin channel (561 nm). Normalization was done by dividing the original standard deviation values by the average control ratio (average of the 3 control fields at t = 0 Min) for each experimental replicate.

Statistical analysis

The number of events per experiment used for statistical analysis is indicated in figure legends. Graphs were created and statistical analysis were done using GraphPad Prism software. P-values were calculated using two-tailed Student's t-tests or Mann Whitney tests.

Acknowledgments

We are grateful to D. Portran from the Liakopoulos team for providing reagents; to members of the Delaval and Liakopoulos team for fruitful discussions. This work was supported by the Agence National de la Recherche, grant number ANR-18-CE-0025-01 to BV and grant number ANR-19-CE13-0014 LUCELL to BD and by the Fondation pour la Recherche Médicale, grant number EQU20210301256 to BD. We acknowledge the Biocampus Montpellier Facilities that

contributed to the project: Montpellier Genomic Collection, PIBBS for SEC-MALS analysis and MRI for imaging. PIBBS is supported by the French National Research Agency (ANR-10-INBS-05 FRISBI). MRI, is member of the national infrastructure France-BioImaging supported by the French National Research Agency (ANR-10-INBS-04, «Investments for the future»).

Author contributions

Conceptualization: AG, BD and BV. Investigation: AG, VS, JVD, BD and BV. Methodology: AG, VS, JVD, BD and BV. Supervision: BD and BV. Funding acquisition: BD and BV. Writing BD and BV with inputs from authors.

Conflict of interest

The authors declare no conflict of interest

Figures legends.

Figure 1. HSET directly binds to a minimal IFT52/70 complex

a. Coomassie blue staining of purified GFP-HSET, SNAP-IFT52/SNAP-IFT70 and SNAP-IFT46. Asterisks indicates THE HRV-3C protease used to cleave IFT proteins from their Strep-Tags during purification. **b.** GFP-Trap pull down of IFT52/70 dimer. **c.** GFP-Trap pull down of IFT46 monomer. **d.** SEC-MALS analysis of GFP-HSET alone, IFT 52/70 alone and HSET mixed withIFT52/70. Absorbance at 280 nm is represented with solid lines, MALS data are represented by adjacent crosses. **e.** Silver staining of the peak fractions from the SEC-MALS analysis presented in panel (**d**).

Figure 2. IFT52/70 binding stimulates HSET processive activity through its oligomerization

a. Kymographs representing individual GFP-HSET (0.5 nM) particles moving along GMPCPP stabilized microtubules in absence or presence of IFT52/70 (1nM). **b**. Graph representing the number of processive events of GFP-HSET particles alone or associated to the indicated IFT proteins. Three independent experiments were analyzed. N=132 events in control, 223 in HSET-IFT46and 640 in HSET-IFT52/70. Bars indicate means and error bars S.E.M. ****$P < 0.0001$; unpaired t-test. **c**. Frequency distribution histogram indicating the number of events of processive particles depending on the number of GFP-HSET dimer per particle. **d**. Image of GFP-HSET decoration of microtubules after 2 minutes of incubation with HSET (5 nM) or GFP-HSET (5nM) plus IFT52/70 (10 nM). **e**. Graph representing GFP-HSET fluorescence signal intensity along microtubule length relative to the average signal of GFP-HSET along the lattice of microtubule in control condition. **f**. Graph representing GFP-HSET fluorescence signal intensity at the comet present at microtubule ends relative to the average signal of GFP-HSET along the lattice of microtubule in control condition. Three independent experiments were analyzed. N=111 events in control condition and 115 in HSET-IFT52/70 condition. Bars indicate means and error bars S.E.M. ****$P < 0.0001$; Mann Whitney test.

Figure 3. IFT52/70 binding stimulates HSET bundling and sliding activity

a. Color coded image of free microtubule seeds (orange arrowheads) moving on a microtubule template (white arrowheads) in the presence of HSET (50 nM) or HSET and IFT52/70 (100 nM). The GFP-HSET signal is visualized on those images. Different colors indicate the position of a same seed at different time points. Non-moving seeds appear brightly white. **b**. Graph showing the number of seeds bound to the template. **c**. Graph showing the number of moving seeds per length of template. For **b.** and **c.** each point represents the measure from a single field of view. 16 fields of view from four independent experiments were analyzed for each

condition. Bars indicate means and error bars S.E.M. **d**. Graph representing the distribution of individual microtubule seed speed. Average speed was measured with N=141 for HSET and N=249 for HSET plus IFT52/70 from three independent experiments. **e**. Violin plot of the ratio of GFP-HSET mean fluorescent signal over tubulin mean fluorescent signal intensity on moving seeds. Bars indicate median and quartiles. N=116 for HSET and N=155 for HSET plus IFT52/70 from four independent experiments. $^{**}P < 0.01$; $^{****}P < 0.0001$; Mann Whitney test.

Figure 4. Increased HSET activity upon IFT52/70 binding favors the formation of active microtubule networks

a. Still images from live imaging of GFP-HSET (50 nM) forming contractile microtubule networks in absence or presence of IFT52/70 (100 nM) at 0, 10 and 30 min of incubation. **b**. Graph showing image contrast measurements over time as a readout of microtubule compaction. **c**. Graph showing the slope of the curves extracted from the linear part of the curves in panel (**b**). Points represent the average of a minimum of five independent experiments, errors bars S.E.M. N=27 individual measurements for HSET alone and HSET plus IFT52/70, N=26 for HSET plus IFT46 and N=14 for HSET plus SNAP. $^{*}P < 0.05$; $^{**}P < 0.01$; $^{****}P < 0.0001$; Mann Whitney test. **d**. Representative image of contractile fiber decoration in the tubulin, HSET and IFT52/70 channels in the HSET + IFT52/70 condition at 10 and 30 minutes. The same field of view is represented in the three channels.

Supplementary Figure 1.

a. Images of the field of view from Movies 1, 2 and 3 used to generate the kymographs in Fig. 2a **b.** Dot plot of the fluorescence signal of GFP particle bleaching in one or two steps corresponding to GFP-HSET monomer or dimer, respectively. Bars indicate average signal. **c**. Violin plot of GFP-HSET individual particles fluorescent signal. Bars indicate median and quartiles. N=136 for HSET condition and 644 for HSET-IFT52/70 condition. **d**. Examples of individual GFP-HSET particles reaching microtubule-ends and staying attached to them. In those two examples HSET (0.5 nM) is incubated with IFT52/70 (1 nM). The red asterisks indicate the time when the particles reach the end. **e**. Images of microtubules decorated with GFP-HSET and Kip2-RFP. The two motors accumulate at opposite microtubule ends. Two examples of two different microtubules are presented.

Supplementary Figure 2.

a. Color coded images of free microtubule seeds moving on microtubule template in presence of HSET (50 nM) or HSET with IFT52/70 (100 nM). Those images represent the same fields of view as in Fig. 3a. The tubulin signal is visualized on those images. **b.** Kymographs of sliding

microtubule seeds in the tubulin channel (MT), the HSET channel and the IFT52/70 channel. Overlap of the different channels can be seen for each condition.

Supplementary Figure 3.

Model for IFT52/70 regulation of HSET and its effects on HSET activity as single particles or during microtubule network organization. IFT52/70 binding to HSET stimulates its motors activity (A) and its microtubule minus-end accumulation (B). It also increases HSET microtubule sliding activity (C). Altogether it helps HSET organizing active microtubule network into aster like structures (D). This activity of IFT52/70 on HSET is comparable to the activity of IFT proteins in cells which facilitates the clustering of extra centrosomes through HSET activity (E).

Movie 1. TIRF microscopy movie of GFP-HSETparticle diffusing on microtubules.

The field of view corresponds to Supplementary Fig. 1a. Time interval is 1,4 sec. The movie runs at 60 fps.

Movie 2. TIRF microscopy movie of GFP-HSET- IFT52/70 particle moving processively on microtubules.

The field of view corresponds to Supplementary Fig. 1a. GFP-HSET is visualized on this movie. Time interval is 1,4 sec. The movie runs at 60 fps. Red arrowhead marks the positions of a processive particle at the first time points of the movie.

Movie 3 TIRF microscopy movie of GFP-HSET- IFT52/70 particle moving processively on microtubules.

The field of view corresponds to Supplementary Fig. 1a. IFT52/70 is visualized on this movie. Time interval is 1,4 sec. The movie runs at 60 fps. Red arrowhead marks the positions of a processive particle at the first time points of the movie.

Movie 4. TIRF microscopy movie of a microtubule seed sliding on a microtubule template in presence of GFP-HSET

The field of view corresponds to Fig. 3a. GFP-HSET is visualized on this movie. Time interval is 1 min. The movie runs at 9 fps.

Movie 5. TIRF microscopy movie of a microtubule seed sliding on a microtubule template in presence of GFP-HSET and IFT52/70

The field of view corresponds to Fig. 3a. GFP-HSET is visualized on this movie. Time interval is 1 min. The movie runs at 9 fps.

Movie 6. TIRF microscopy movie of a microtubule seed sliding on a microtubule template in presence of GFP-HSET

The field of view corresponds to Supplementary Fig. 2a. Tubulin is visualized on this movie. Time interval is 1 min. The movie runs at 9 fps.

Movie 7. TIRF microscopy movie of a microtubule seed sliding on a microtubule template in presence of GFP-HSET and IFT52/70

The field of view corresponds to Supplementary Fig. 2a. Tubulin is visualized on this movie. Time interval is 1 min. The movie runs at 9 fps.

Movie 8. Wide field epifluorescence microscopy movie of an active microtubule network organizing over time upon the activity of GFP-HSET.

The field of view corresponds to Fig. 4a. Tubulin is visualized on this movie. Time interval is 1,5 min. The movie runs at 10 fps.

Movie 9. Wide field epifluorescence microscopy movie of an active microtubule network organizing over time upon the activity of GFP-HSET with IFT52/70.

The field of view corresponds to Fig. 4a. Tubulin is visualized on this movie. Time interval is 1,5 min. The movie runs at 10 fps.

Figure 1

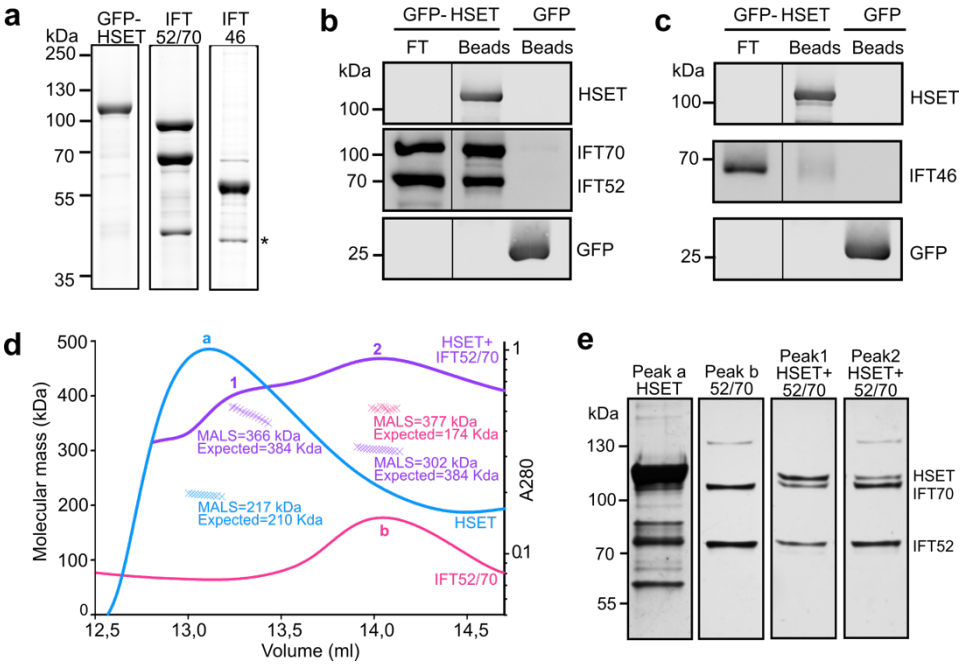
a
kDa
GFP-HSET
IFT 52/70
IFT 46
250
130
100
70
55
35
*
b
GFP-HSET
GFP
FT
Beads
Beads
kDa
100
HSET
100
70
IFT70
IFT52
25
GFP
c
GFP-HSET
GFP
FT
Beads
Beads
kDa
100
HSET
70
IFT46
25
GFP
d
Molecular mass (kDa)
500
400
300
200
100
0
12,5
13,0
13,5
14,0
14,5
Volume (ml)
a
1
2
HSET+ IFT52/70
MALS=366 kDa Expected=384 Kda
MALS=377 kDa Expected=174 Kda
MALS=302 kDa Expected=384 Kda
MALS=217 kDa Expected=210 Kda
HSET
b
IFT52/70
A280
1
0.1
e
Peak a HSET
Peak b 52/70
Peak1 HSET+ 52/70
Peak2 HSET+ 52/70
kDa
130
100
70
55
HSET
IFT70
IFT52

Figure 2

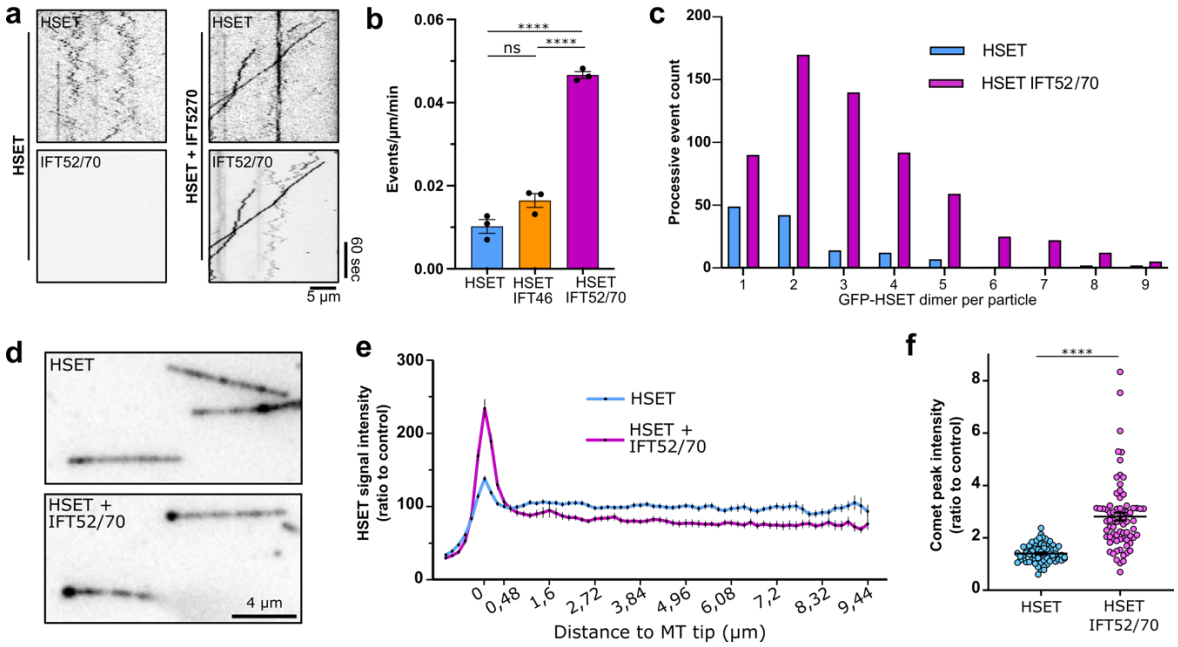
a
HSET
HSET
IFT52/70
HSET + IFT5270
HSET
IFT52/70
60 sec
5 µm
b
Events/µm/min
0.06
0.04
0.02
0.00
****
ns
****
HSET
HSET IFT46
HSET IFT52/70
c
Processive event count
200
150
100
50
0
HSET
HSET IFT52/70
1
2
3
4
5
6
7
8
9
GFP-HSET dimer per particle
d
HSET
HSET + IFT52/70
4 µm
e
HSET signal intensity (ratio to control)
300
200
100
0
HSET
HSET + IFT52/70
0
0,48
1,6
2,72
3,84
4,96
6,08
7,2
8,32
9,44
Distance to MT tip (µm)
f
Comet peak intensity (ratio to control)
8
6
4
2
0
****
HSET
HSET IFT52/70

Figure 3

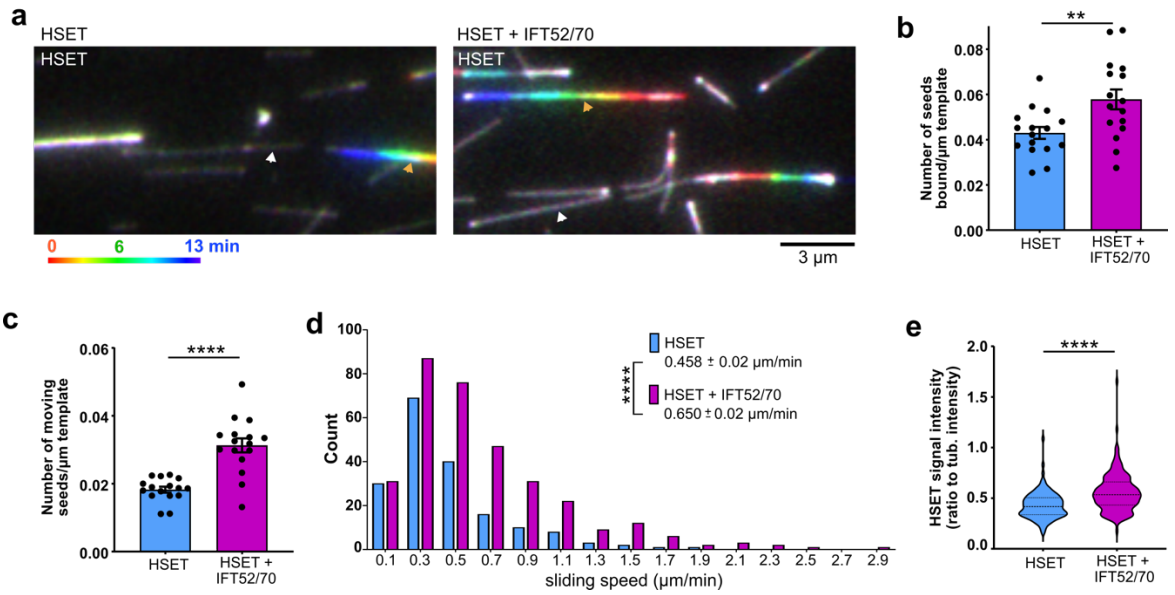
a
HSET
HSET
HSET + IFT52/70
HSET
0
6
13 min
3 µm
b
**
Number of seeds bound/µm template
0.08
0.06
0.04
0.02
0.00
HSET
HSET + IFT52/70
c
****
Number of moving seeds/µm template
0.06
0.04
0.02
0.00
HSET
HSET + IFT52/70
d
Count
100
80
60
40
20
0
HSET
0.458 ± 0.02 µm/min
****
HSET + IFT52/70
0.650 ± 0.02 µm/min
0.1 0.3 0.5 0.7 0.9 1.1 1.3 1.5 1.7 1.9 2.1 2.3 2.5 2.7 2.9
sliding speed (µm/min)
e
****
HSET signal intensity (ratio to tub. intensity)
2.0
1.5
1.0
0.5
0.0
HSET
HSET + IFT52/70

Figure 4

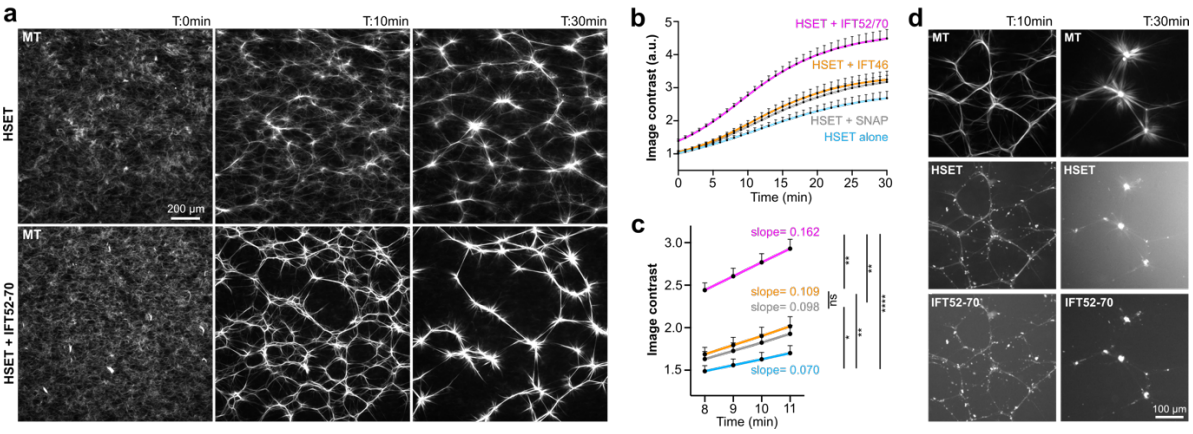
a
T:0min
T:10min
T:30min
MT
HSET
200 µm
HSET + IFT52-70
b
HSET + IFT52/70
HSET + IFT46
HSET + SNAP
HSET alone
Image contrast (a.u.)
Time (min)
c
slope= 0.162
slope= 0.109
slope= 0.098
slope= 0.070
Image contrast
Time (min)
NS
d
T:10min
T:30min
MT
HSET
IFT52-70
100 µm

Supplementary Fig. 1

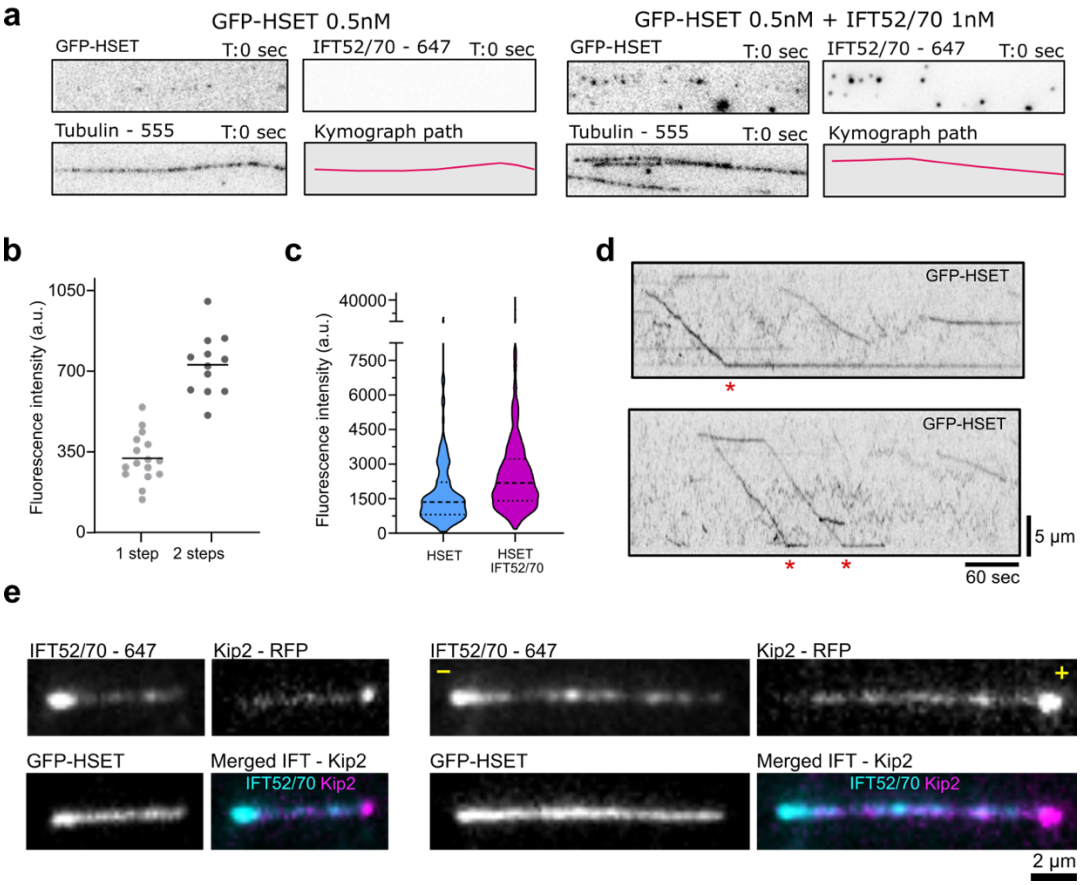

Supplementary Fig. 2

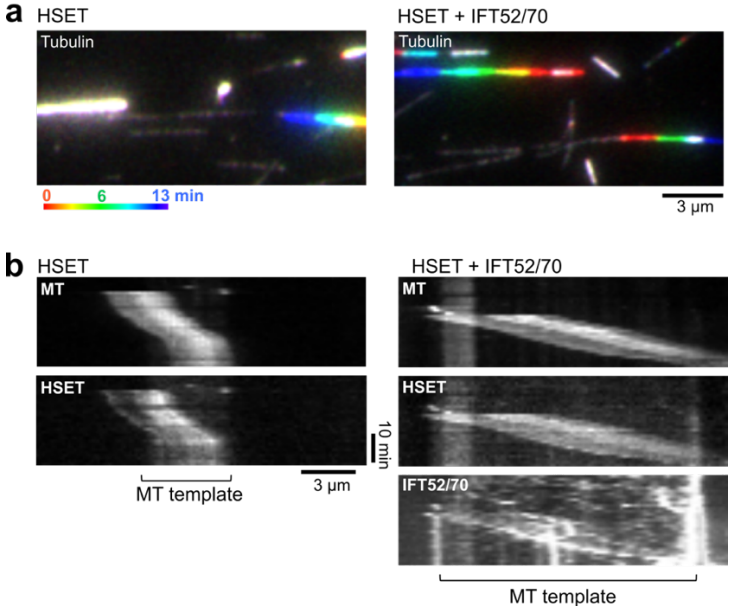
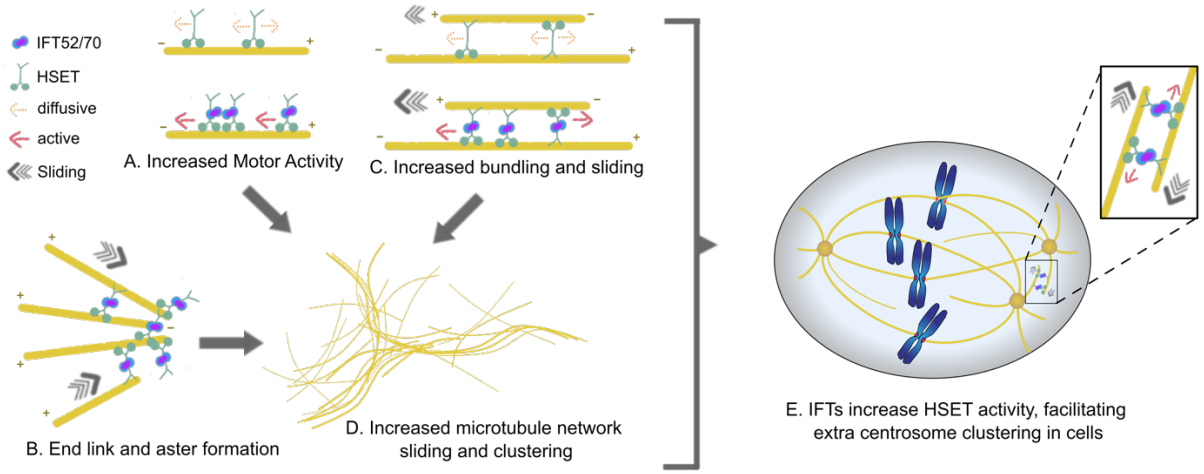
Supplementary Figure 3